Transient chaos and associated system-intrinsic switching of spacetime patterns in two synaptically coupled layers of Morris-Lecar neurons

Harrison Hartle* and Renate Wackerbauer†
Department of Physics, University of Alaska, Fairbanks, Alaska 99775-5920, USA
(Received 30 January 2017; published 20 September 2017)

Spatiotemporal chaos collapses to either a rest state or a propagating pulse solution in a single layer of diffusively coupled, excitable Morris-Lecar neurons. Weak synaptic coupling of two such layers reveals system intrinsic switching of spatiotemporal activity patterns within and between the layers at irregular times. Within a layer, switching sequences include spatiotemporal chaos, erratic and regular pulse propagation, spontaneous network wide neuron activity, and rest state. A momentary substantial reduction in neuron activity in one layer can reinitiate transient spatiotemporal chaos in the other layer, which can induce a swap of spatiotemporal chaos with a pulse state between the layers. Presynaptic input maximizes the distance between propagating pulses, in contrast to pulse merging in the absence of synapses.

DOI: 10.1103/PhysRevE.96.032223

I. INTRODUCTION

The concept of transient dynamics is crucial for the understanding of real systems [1]. Transient brain activity is reported, e.g., in perception associated with stimuli [2], as disruption of neurological rhythms in seizure [3,4], and in migraine attacks [5]. Prevalent mechanisms for abrupt changes in system dynamics include parameter perturbation near bifurcations [6], noise in the presence of attractors [7], deterministic transients near heteroclinic orbits [8], and transient stable chaos [9–11].

Transient spatiotemporal chaos presents an abrupt change from chaotic extended dynamics to regular behavior, typically associated with the existence of a chaotic saddle, i.e., an invariant manifold that is not attractive [1,12]. Turbulence in shear flow experiments is transient [13]. Spatiotemporal chaos is transient in excitable reaction diffusion models for semiconductor charge transport [14], for chemical reactions [15,16], and for coupled Morris-Lecar neurons [17]; the complex Ginzburg-Landau equation exhibits a collapse of spatiotemporal chaos to an oscillatory medium [18].

Transient spatiotemporal chaos is extensive [15,19–22], which explains the exponential increase of its average lifetime with system size [12,14–16] based on the probability of uncorrelated local regions generating a global pattern that initiates the collapse [23]. The finite lifetimes can be manipulated by noise [24], the addition of nonlocal coupling in the network topology [25,26], and can become asymptotic when adding competition between chaotic populations [27].

Complex networks frequently exhibit dynamically connected saddles via heteroclinic connections [8,28,29]. A typical trajectory reveals sustained switching between such metastable states until an attractor is reached. Specific switching sequences reliably encode information and are discussed for computation [30]. A control strategy was recently devised and explored in pulse-coupled oscillator networks, to sustain the switching dynamics by preventing the escape to an attractor [31]. These studies on switching behavior involve simple saddles, where the invariant manifold is typically a point or a limit cycle. A chaotic saddle is involved in the alternating dynamics between transient spatiotemporal chaos and traveling pulse in a network of diffusively and synaptically coupled excitable Morris-Lecar neurons [26]. A more complicated chaotic saddle was identified in a large, two-dimensional (small world) network of coupled nonidentical, oscillatory FitzHugh-Nagumo neurons with local coupling neighborhood [32]. An irregular switching between low-amplitude oscillations, waves, and extreme events was observed and associated with a single chaotic saddle that contains these three space-time patterns that are connected via channel-like structures to mediate the switching.

This paper numerically explores the switching of spatiotemporal patterns associated with a chaotic saddle in a system of two synaptically coupled layers of identical, excitable Morris-Lecar neurons. Section II introduces the model and briefly summarizes transient spatiotemporal chaos in a single layer. Observed sequences of switching are discussed in Sec. III for (one-way) synaptic coupling from one layer to the other layer. Section IV shows preliminary results for switching behavior observed in two-way synaptic coupling between the layers. Conclusions are presented in Sec. V.

II. MODEL

The system consists of two synaptically coupled layers of identical, excitatory Morris-Lecar (ML) neurons [33,34]. Each layer represents a ring network of N diffusively coupled ML neurons. The synapse topology is fully connected such that each neuron in one layer is synaptically coupled to every neuron in the other layer. The state of neuron i (with $i = 1,\ldots,N$) in layer k (with $k = \mathrm{I,II}$) is given by the membrane potential, V_i^k, and the fraction of open potassium channels, n_i^k:

$$\begin{aligned}\dot{V}_i^k &= \frac{1}{C_\mathrm{m}}\left(I - I_i^{\mathrm{ion},k} - I_i^{\mathrm{syn},k}\right) + D\Delta_i^k,\\ \dot{n}_i^k &= \tau_i^k\left(n_i^{\mathrm{ss},k} - n_i^k\right),\end{aligned} \tag{1}$$

with membrane capacitance C_m, applied current I, ionic current I^{ion}, and synaptic current I^{syn} (per unit area). n^{ss} is the fraction of open potassium channels at steady state and

*hthartle@alaska.edu
†rawackerbauer@alaska.edu

TABLE I. Model parameters for the (class I) ML neuron [33,34], for the synaptic coupling with AMPA receptor [35–37], and transient spatiotemporal chaos [17,26].

$I = 32\ \mu\text{A/cm}^2$	$D = 0.05\ \text{ms}^{-1}$	$C_\text{m} = 20\ \mu\text{F/cm}^2$
$g_\text{K} = 8\ \text{mS/cm}^2$	$g_\text{L} = 2\ \text{mS/cm}^2$	$g_\text{Ca} = 4\ \text{mS/cm}^2$
$V_\text{K} = -80\ \text{mV}$	$V_\text{L} = -60\ \text{mV}$	$V_\text{Ca} = 120\ \text{mV}$
$V_1 = -1.2\ \text{mV}$	$V_2 = 18\ \text{mV}$	$V_3 = 14.95\ \text{mV}$
$V_4 = 17.4\ \text{mV}$	$\varphi = 1/15\ \text{s}^{-1}$	$V_\text{s} = 0\ \text{mV}$
$\alpha = 1.1\ \text{mM}^{-1}\ \text{ms}^{-1}$	$\beta = 0.19\ \text{ms}^{-1}$	$T_\text{m} = 1.0\ \text{mM}$
$V_\text{p} = 2.0\ \text{mV}$	$K_\text{p} = 5.0\ \text{mV}$	

τ determines the time constant for opening/closing of potassium channels. The electrical coupling between neighboring neurons in, e.g., axo-axonic gap junction networks [38,39], is modeled with the diffusion operator, $\Delta_i^k = V_{i-1}^k + V_{i+1}^k - 2V_i^k$, and D is the diffusive coupling strength. All (fixed) model parameters are summarized in Table I.

The ionic current, I^ion, considers the inward calcium current, the outward potassium current, and the leak current that is associated with other ion fluxes across the membrane:

$$I_i^{\text{ion},k} = g_\text{Ca} m_i^{\text{ss},k}\left(V_i^k - V_\text{Ca}\right) + g_\text{K} n_i^k\left(V_i^k - V_\text{K}\right) + g_\text{L}\left(V_i^k - V_\text{L}\right), \tag{2}$$

with leak conductance g_L, leak resting potential V_L, maximum calcium conductance g_Ca and potassium conductance g_K, and reversal potential for the calcium current V_Ca and for the potassium current V_K. The fraction of open calcium (potassium) channels at steady state, m^ss (n^ss), and the inverse time scale for potassium channel opening, τ, are given by

$$m_i^{\text{ss},k} = \frac{1}{2}\left[1 + \tanh\left(\frac{V_i^k - V_1}{V_2}\right)\right], \tag{3}$$

$$n_i^{\text{ss},k} = \frac{1}{2}\left[1 + \tanh\left(\frac{V_i^k - V_3}{V_4}\right)\right], \tag{4}$$

$$\tau_i^k = \varphi\,\cosh\left(\frac{V_i^k - V_3}{2V_4}\right). \tag{5}$$

The synaptic current for neuron i in network k [Eq. (1)] is modeled as an ohmic current [35,37],

$$I_i^{\text{syn},k} = g \sum_{\substack{l=\text{I} \\ l\neq k}}^{\text{II}} \sum_{j=1}^{N} w_{ji}^{lk} s_{ji}^{lk}\left(V_i^k - V_\text{s}\right), \tag{6}$$

where g is the conductance of the synapse and w_{ji}^{lk} represents the synaptic coupling tensor. w_{ji}^{lk}=1, if there exists a synaptic link from presynaptic neuron j in layer l to the post synaptic neuron i in layer k, otherwise $w_{ji}^{lk} = 0$. Since synaptic coupling is absent within each layer, $w_{ji}^{lk} = 0$ for $l = k$; in other words, $l \neq k$ in Eq. (6). This study focuses on fully coupled, synaptic projections from layer I (input layer) to layer II (output layer), where every input neuron in layer I is synaptically coupled to every output neuron in layer II (*one-way synaptic coupling*). In this case, $w_{ji}^{\text{I,II}} = 1$ and $w_{ji}^{\text{II,I}} = 0$ for all i, j, and $I_i^{\text{syn,I}} = 0$ for all input neurons i. Preliminary results are also given for bidirectional, synaptic projections between the two layers, where every neuron in each layer is synaptically coupled to every neuron in the other layer, $w_{ji}^{\text{II,I}} = w_{ji}^{\text{I,II}} = 1$ (*two-way synaptic coupling*). s_{ji}^{lk} is the fraction of open channels in the synaptic cleft between presynaptic neuron j in layer l and postsynaptic neuron i in layer k, and V_s is the reversal potential of the channel. The fraction of open channels is given by

$$\dot{s}_{ji}^{lk} = \frac{\alpha\left(1 - s_{ji}^{lk}\right)T_\text{m}}{1 + \exp\left(-\frac{(V_j^l - V_\text{p})}{K_\text{p}}\right)} - \beta s_{ji}^{lk}. \tag{7}$$

α and β are growth and decay rate constants, respectively. The parameters T_m, V_p, and K_p (Table I) and the membrane voltage of the presynaptic neuron, V_j^l, determine the sigmoidal shape of the neurotransmitter concentration in the synaptic cleft.

A bifurcation analysis for a single ML neuron [17,34] [$D = 0$, $g = 0$ in Eq. (1)] reveals an excitable neuron for applied currents, I, below the saddle-node on invariant circle (SNIC) bifurcation point at $I = 38.7\ \mu\text{A/cm}^2$. In this excitable regime the neuron dynamics is characterized by three steady states, a stable node (rest state), a saddle point, and an unstable focus. A superthreshold perturbation to the rest state causes an excitation cycle [Fig. 1(a)], where a typical trajectory moves further away from the rest state and passes the unstable focus before returning to the rest state. A ring network (layer) of diffusively coupled ML neurons is excitable, if the excitation can spread between neurons. A numerical analysis shows that excitation propagation exists for applied currents above $I = 28.1\ \mu\text{A/cm}^2$. In the parameter regime between the onset of excitation propagation and the SNIC bifurcation point, a network of diffusively coupled neurons exhibits transient spatiotemporal chaos [17,26]. We use a representative, intermediate value of $I = 32\ \mu\text{A/cm}^2$ in this paper.

An isolated layer [$g = 0$ in Eq. (1)] of diffusively coupled neurons exhibits transient spatiotemporal chaos [17,26] with an average lifetime that grows exponentially with network size, typical for reaction-diffusion systems [12,16,19,40]. During the transient phase the diffusive coupling sustains neuron excitations to yield a complex, irregular spatiotemporal pattern with chaotic dynamics [Figs. 1(b) and 1(c)]. Inactive neuron groups with trajectories close to or at their stable node (dark patches) alternate with active neuron groups where trajectories spiral around the unstable focus. A typical neuron's trajectory for the chaotic dynamics is plotted in Fig. 1(a). The spatiotemporally chaotic dynamics eventually collapses abruptly to either the rest state [Fig. 1(b)], where every neuron is at its stable node, or to a state with one or more coexisting traveling pulses [Fig. 1(c)]. Two types of pulses are observed, a *wide pulse* and a *narrow pulse*, which differ in their pulse profiles [Fig. 1(d)] and in their phase portraits. A master stability analysis [40] shows that the rest state is attractive, and long-term numerical simulations reveal that each single pulse is stable in the absence of synaptic coupling [17,26]. The spontaneous, system intrinsic collapse points to the existence of a chaotic saddle as a result of the coexisting regular attractors [12]. The lifetimes of transient spatiotemporal chaos do not differ significantly from each other whether the collapse is to the rest state or to the pulse solution. This is expected if one assumes a single nonattracting chaotic set, which implies the

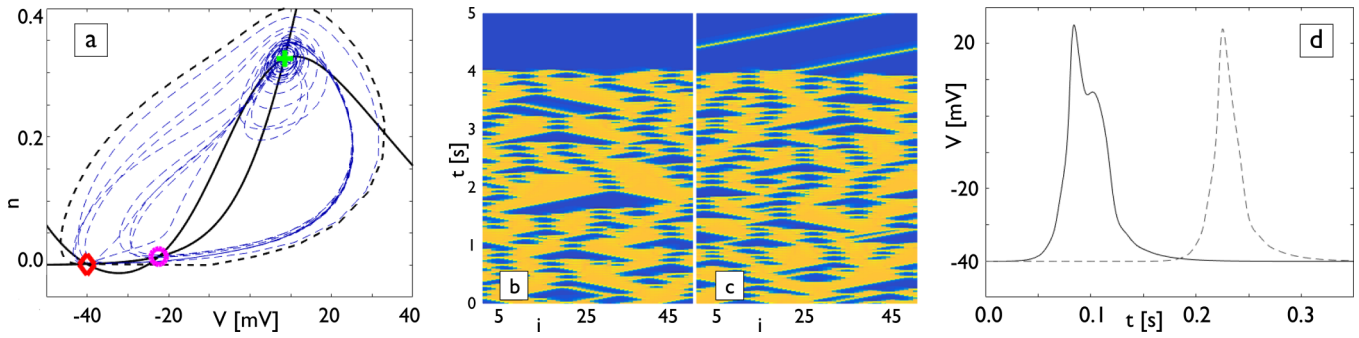

FIG. 1. (a) A typical excitation cycle in phase space for a single ML neuron (thick dashed line) and a typical trajectory of a coupled neuron with chaotic dynamics (thin dashed line). The cubic V-nullcline and the n-nullcline (full lines) are shown, together with the three steady states, a stable node (diamond), a saddle point (circle), and an unstable focus (plus). Typical examples of spatiotemporal dynamics of the membrane potential (V) for a diffusively coupled ML network ($g = 0, N = 50$) when spatiotemporal chaos collapses to (b) the global rest state, and to (c) a traveling pulse solution. A membrane potential (V) close to the rest state (unstable focus) is represented in dark (lighter) color. The plotted time interval reflects the dynamics near the time of collapse. The simulations were started with a superthreshold perturbation $(V,n) = (-10\ \text{mV},0)$ of a single neuron, with all other neurons in the rest state. More details on generic initial conditions that reach the neighborhood of the chaotic saddle are presented in Keplinger *et al.* [17]. (d) Comparison of narrow (dashed line) and wide (solid line) pulse solution via their time evolution of the membrane potential V. The phase portraits of these two pulses are depicted in Fig. 8.

same escape probability from the neighborhood of the chaotic saddle to either of the attractors.

III. SWITCHING OF PATTERNS IN A SYSTEM WITH ONE-WAY SYNAPTIC COUPLING FROM LAYER I TO LAYER II

Two identical layers of neurons are one-way, fully synaptically coupled such that every input neuron in layer I is synaptically coupled to every output neuron in layer II, according to Eq. (1). Each layer consists of a diffusively coupled ring network of N identical excitatory ML neurons that is initially in the state of transient spatiotemporal chaos (STC). Layer I is not influenced by the synapses and the escape dynamics from the neighborhood of the chaotic saddle is identical to the one in the isolated, diffusive ring network studied in Refs. [17,26]. The dynamics in layer II is synaptically driven by layer I; it also exhibits a collapse from chaotic dynamics to the rest state or to diverse pulse states.

Figure 2 shows two representative switching sequences from an initially STC state in both layers to an asymptotic system state. While layer I is in an STC state, the dynamics in layer II switches from STC to a stripe pattern, where all neurons within the layer are simultaneously excited at irregular times. Eventually, STC in layer I collapses to a narrow pulse, and the stripe pattern switches into a state where all neurons are inactive. In the second example [Fig. 2(b)], STC in layer II switches into an erratic pulse pattern. When the dynamics in layer I collapses from STC to a traveling wide pulse, STC is simultaneously reinitiated in layer II. After some transient time, STC in layer II collapses to a narrow pulse, and the asymptotic system state is reached. Figure 3 shows an overview of observed system intrinsic switching patterns for weak synaptic coupling ($g = 0.01\ \text{mS/cm}^2$) and an initially STC state in both layers. Each transition is discussed individually in the following sections.

This study focuses on weak synaptic coupling, fixed at $g = 0.01\ \text{mS/cm}^2$, except in few cases where g is varied to demonstrate the robustness of a phenomenon or to provide further insight. This coupling is small enough that traveling (narrow, wide) pulses in layer I cannot excite a postsynaptic neuron from rest (Fig. 4), but a fully active input layer in the state of spatiotemporal chaos eventually can.

A. Chaos in layer I, stripe pattern in layer II

A simultaneous excitation of all postsynaptic neurons at aperiodic moments in time [stripe pattern, Fig. 2(a)] is observed when transient spatiotemporal chaos collapses to the rest state in layer II while still active in layer I. Synaptic projections from layer I influence all postsynaptic neurons equally and eventually cause a network wide excitation [41], if the coupling strength is above the critical coupling strength for neuron excitation from the rest state (case A, Fig. 4). The stripe pattern persists as long as spatiotemporal chaos is existent in layer I; it suddenly terminates when STC collapses to the rest state or to any of the traveling pulse states. The average lifetime of the stripe pattern is 170.6 ± 181.8 s (determined from the 30 instances of stripe formation in 100 simulations, $g = 0.01\ \text{mS/cm}^2$), which is larger than the average lifetime of STC in layer I, 131.0 ± 136.4 s (100 simulations), since it excludes short lifetimes where STC in I collapsed before stripe formation in layer II. Synaptic projections also influence the escape statistics from the chaotic saddle, decreasing the likelihood for collapse to rest and thus for collapse to a stripe pattern with increasing g. Collapse to rest is observed in 56% of simulations for an isolated diffusive ring network ($g = 0$), and in 50%, 40%, 30% of simulations with synaptic input of strength $g = 0.010,\ 0.020,\ 0.025\ \text{mS/cm}^2$.

Figures 5(a) and 5(b) contrast STC in layer I with the stripe formation in layer II for different coupling strengths g. Weaker synapses lead to a later onset of stripe formation and to the omission of some of the stripes. No stripes are formed below a critical synapse strength. The rate of stripe formation increases with synapse strength g [Fig. 5(c)]; for large enough coupling, postsynaptic neurons are always active and stripes no longer exist.

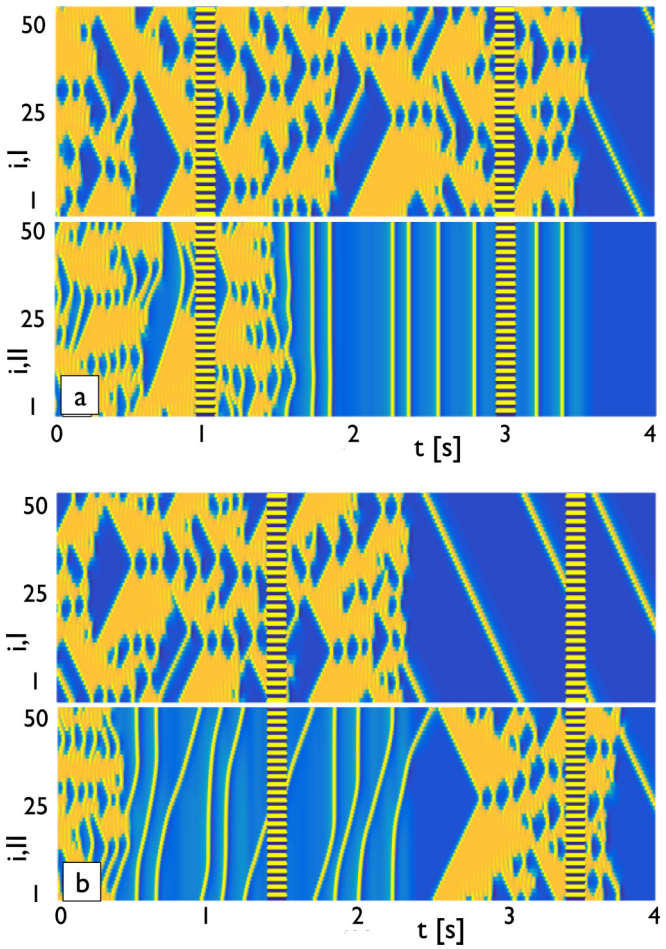

FIG. 2. Typical system intrinsic switching sequences of spatiotemporal patterns in layers I and II, initially in the STC state. The synaptic coupling is one-way, from layer I to II, with standard coupling, $g = 0.01$ mS/cm^2. Panels (a) and (b) differ by randomly chosen initial conditions. The vertical lines indicate a break in time. Times are given only to illustrate the time scale within a pattern. For other parameters, see Fig. 1(b).

Stripes are formed when the synaptic input forces the postsynaptic neuron trajectory to cross the nullcline (Fig. 1) to cause an excitation. The postsynaptic neuron is initially (after the collapse of STC) in the rest state (stable node), where the membrane potential is negative. The corresponding negative synaptic current, $I_i^{\mathrm{syn,II}} = g V_i^{\mathrm{II}} \sum_{j=1}^{N} s_{ji}^{\mathrm{I,II}}$ [rewritten from Eq. (6)], adds a positive growth term to the membrane potential [Eq. (1), $\Delta_i^{\mathrm{II}} = 0$ in the absence of gradients], and the postsynaptic neuron's trajectory is governed by a competition between deviations from rest state toward larger membrane potential and the attraction toward the stable rest state. For synapse strengths below the critical value for excitation, the corresponding fluctuations of the trajectory away and back toward the rest state never terminate. For weak synapse strengths (e.g., $g = 0.01$ mS/cm^2), the trajectory eventually crosses the threshold to initiate an excitation cycle. For stronger synapses the synaptic current is more negative to easier reach that threshold.

Figure 6 shows the time series of the synaptic current, the postsynaptic neuron's membrane potential, and the presynaptic

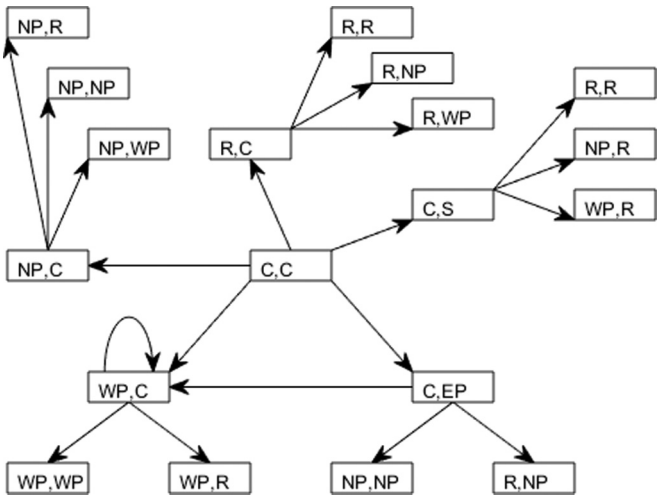

FIG. 3. Summary sketch for switching behavior in the case of one-way synaptic coupling from layer I to II and synapse strength, $g = 0.01$ mS/cm^2. The notation [A, B] refers to state A in layer I and state B in layer II with following abbreviations C (STC), WP (wide pulse), NP (narrow pulse), EP (erratic pulse), S (stripe pattern), and R (rest state). Final states are asymptotic, and arrows mark state transitions. The collapse to multiple pulses is ignored.

input ($I_p = g \sum_{j=1}^{N} s_{ji}^{\mathrm{I,II}}$) during the stripe pattern of the simulation in Fig. 5(a) for weak synapse strength. During larger time intervals between successive excitations, the described fluctuations of the trajectory are visible in the membrane potential, during shorter time intervals between excitations there is a steady increase of the membrane potential to reach and cross the threshold for excitation initiation. Moments of excitation do not correlate with peaks in the presynaptic input; the required nullcline crossing for an excitation event is

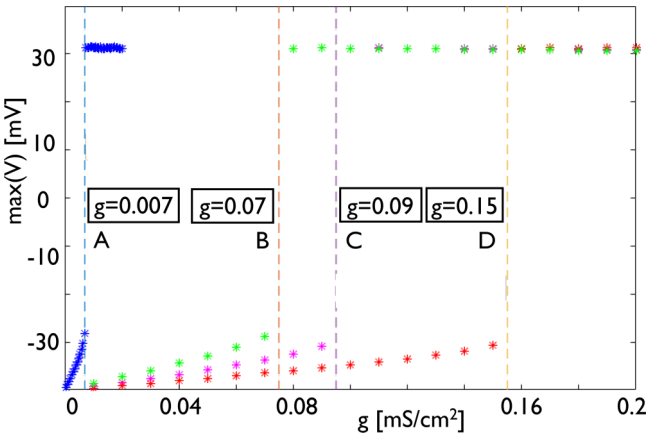

FIG. 4. Maximum membrane potential, max(V), of a postsynaptic neuron (layer II) versus synaptic coupling strength g, if the input layer of $N = 50$ neurons exhibits spatiotemporal chaos (A), two traveling narrow pulses (B), a single traveling wide pulse (C), or a single traveling narrow pulse (D). The critical coupling strengths for the excitation of a postsynaptic neuron from the rest state are marked as vertical lines; they are clearly below $g = 1.5$ mS/cm^2, for which a single active presynaptic neuron can excite a postsynaptic neuron in the rest state and thus trivially keep layer II active.

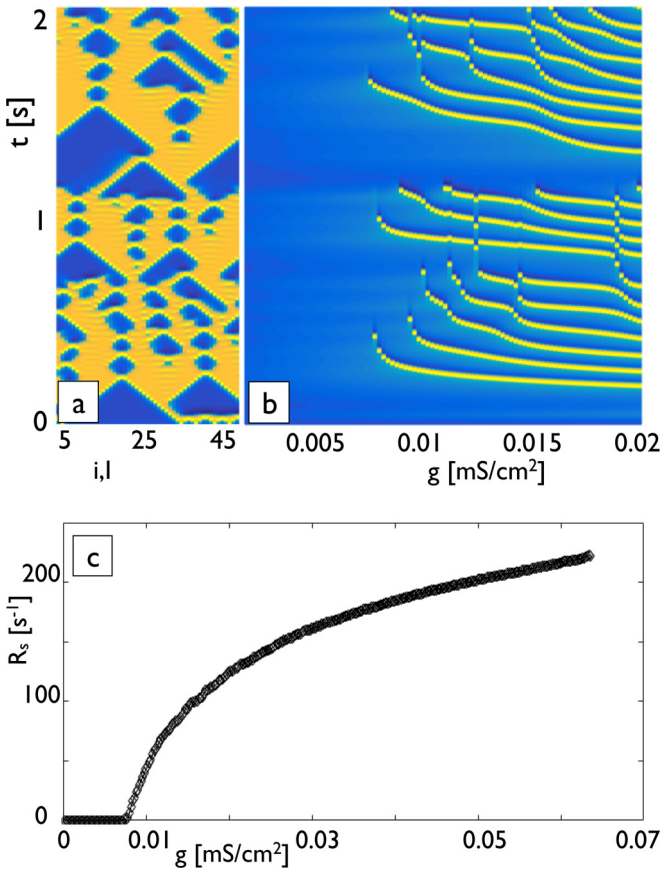

FIG. 5. (a) Spatiotemporal chaos in layer I, and (b) corresponding stripe locations in layer II as a function of synaptic coupling g. (c) The rate R_s (number of stripes per 200 s) at which a chaotic input layer generates stripes in the output layer as a function of coupling strength g. Stripe patterns are absent for stronger synaptic coupling, since neurons in layer II are continuously excited.

achieved via diverse combinations of smaller and/or larger presynaptic inputs. The presynaptic input resembles the number of excited presynaptic neurons at any given time [42].

B. Chaos in layer I, single erratic pulse in layer II

An erratic pulse pattern (Fig. 7) is observed when transient spatiotemporal chaos collapses to a (wide or narrow) traveling pulse state in layer II while persisting in layer I. The percentage for such collapse to either pulse state is 36% for weak synaptic coupling ($g = 0.01$ mS/cm^2) and 42% for an isolated diffusive ring network ($g = 0$). The erratic pulse exhibits a range of propagation speeds along the ring network due to the irregular synaptic input, which implies a range of trajectories in phase space that slightly differ from the wide and narrow pulse (Fig. 8). The erratic pulse pattern terminates when STC in layer I collapses: A collapse to the rest state ceases the synaptic input and the erratic pulse becomes the narrow pulse of the diffusive system, which is an asymptotic state. A collapse to the narrow traveling pulse causes a constant synaptic input for layer II, and the erratic pulse switches into the asymptotic state of a (driven) uniformly traveling narrow pulse [45]; the (driven) narrow pulse in layer II travels faster than the narrow pulse in layer I, and its phase space trajectory is close to that of

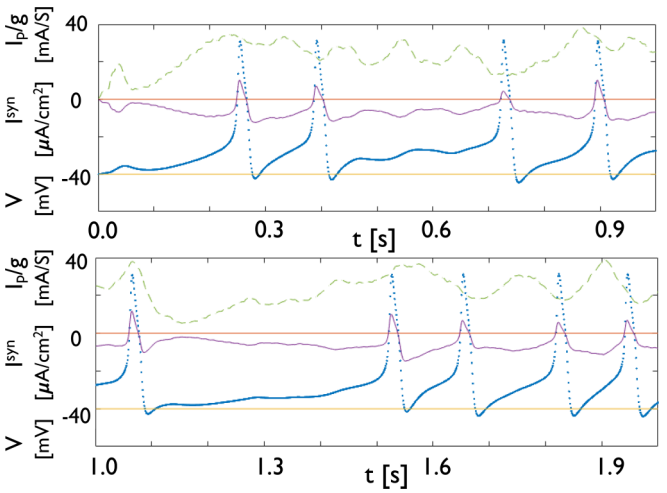

FIG. 6. Time series of presynaptic input ($I_p = g\sum_{j=1}^{N} s_{ji}^{\mathrm{I,II}}$, dashed line), synaptic current ($I_i^{\mathrm{syn,II}}$, full line), and membrane potential (V_i^{II}, dotted line) of postsynaptic neuron (i) for the simulation in Fig. 5(a) with synapse strength $g = 0.01$ mS/cm^2. The horizontal lines mark the zero line and the membrane potential in the rest state.

the narrow pulse. The phase space trajectories of the various pulses are plotted in Fig. 8. The case when STC in network I collapses to a wide pulse yields a nonasymptotic state and is discussed in Sec. III E.

The erratic nature of the pulse stems from its varying propagation speed superimposed with the generation of stripelike excitation patterns. The stripelike parts exist at the same time when the synaptic input would generate a stripe if network II were in the rest state (Fig. 7). As the erratic pulse travels along the network with its instantaneous speed, it experiences times when the presynaptic input excites all excitable postsynaptic neurons. Postsynaptic neurons in the wake of the traveling pulse are in a refractory state and cannot be excited, which adds

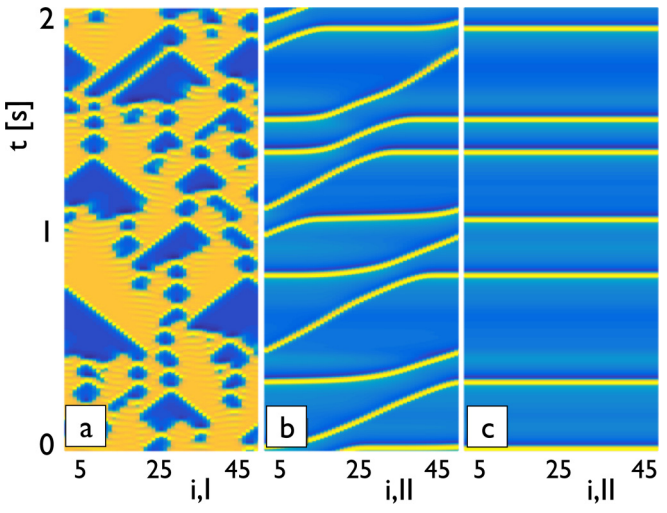

FIG. 7. (a) Spatiotemporal chaos in layer I and (b) corresponding erratic pulse pattern in layer II. (c) The stripe pattern (Sec. III A) initiated from layer I is plotted for comparison. The synapse strength is $g = 0.01$ mS/cm^2.

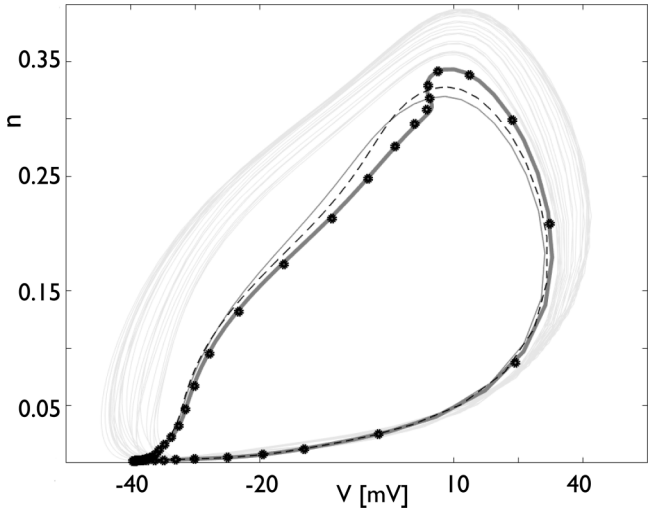

FIG. 8. Phase space trajectories of a narrow pulse (full line), a (driven) narrow pulse (dashed line), a wide pulse (bold full line), a (driven) wide pulse (circles), and an erratic pulse (light colored full line). The narrow and wide pulse refer to pulse solutions in a diffusive layer without synaptic input [see also Fig. 1(d)]. The (driven) narrow/wide pulse experiences synaptic input from layer I ($g = 0.01\,\mathrm{mS/cm^2}$), in this case from a narrow pulse in layer I; the (driven) narrow/wide pulse becomes the narrow/wide pulse upon termination of the synaptic input. The erratic pulse develops from any pulse that experiences synaptic input from STC; the erratic pulse becomes a narrow pulse upon termination of the synaptic input.

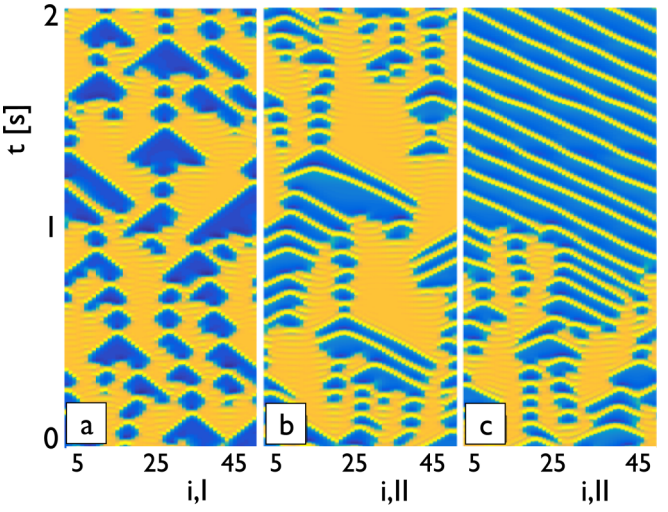

FIG. 9. Spatiotemporal chaos in (a) layer I and (b) layer II. (c) An example for STC collapsing to four erratic pulses in layer II. The synaptic strength is $g = 0.01\,\mathrm{mS/cm^2}$.

an interruption to the stripe pattern. As time progresses, the refractory neurons farthest in the wake of the original traveling pulse become excitable first and their diffusive interaction with the neighboring active neuron starts a new (delayed) pulse traveling in the direction of the newly excitable (nonrefractory) neurons.

C. Spatiotemporal chaos in layers I and II

During transient times without collapse, STC in layer II is altered relative to STC in layer I by the synaptic input. Figure 9 reveals more frequent and often repetitive *internal pulses*; activity with small spatial and temporal scale is propagating through groups of inactive neurons in certain parts of the ring network. These repetitive internal pulses lead to an increased probability for collapse to multiple pulses. Figure 9(c) shows a rare example in a 50-neuron output layer, where STC collapses to four erratic pulses. The repetitive internal pulses on subnetwork scale appear to precede the traveling erratic pulses.

Figure 10 shows that the largest Lyapunov exponent is positive for a range of coupling strengths and how the average lifetime $\langle T \rangle$ of transient STC in layer II is influenced by the synaptic input. STC is collapsing fastest for weak synapses at $g = 0.010\,\mathrm{mS/cm^2}$. Beyond that strength, a gradual and then steep increase in transient lifetime is observed. Trial simulations for $g = 0.030\,\mathrm{mS/cm^2}$ did not reveal any collapse, even on time scales that are an order of magnitude larger than the biggest $\langle T \rangle$ in Fig. 10(b). This may not imply asymptotic STC, since inactive neuron groups up to half the network size have been observed few times; the collapse of STC to pulse or rest state, however, requires almost all or all neurons being inactive, which is expected to be an extremely rare event. The fast collapse at $g = 0.010\,\mathrm{mS/cm^2}$ correlates with more frequent internal pulse patterns in STC (Fig. 9) and a faster collapse to pulse; half of the simulations show a collapse to pulse with an average transient lifetime of 19.6 ± 18.0 s, while

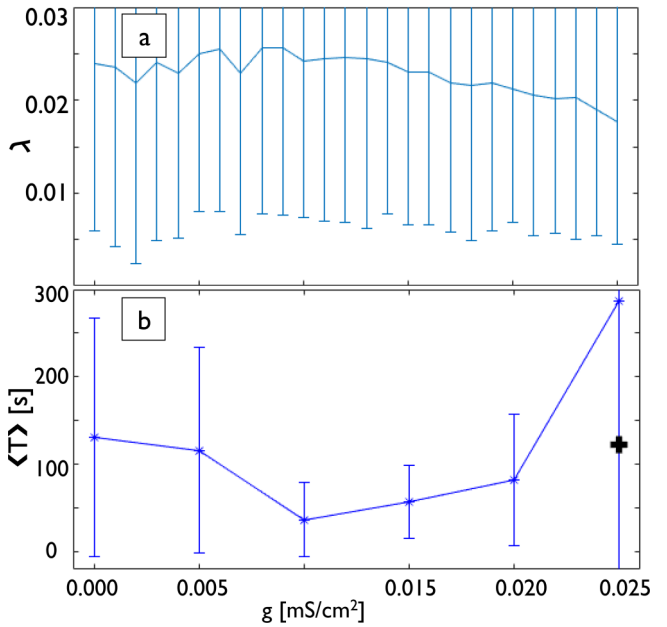

FIG. 10. (a) Largest Lyapunov exponent λ [26,46] and (b) average lifetime $\langle T \rangle$ of transient STC in layer II versus synaptic coupling strength g when layer I is in the STC state. Error bars (one standard deviation) are plotted where scale allows; half standard deviation is marked for the last data point (+). The average is over 50 simulations with different initial conditions, a combination of 10 (5) randomly chosen STC initial conditions in layer II (I). The distribution of lifetimes for each data point (not plotted) appears exponential, consistent with other studies [12,16].

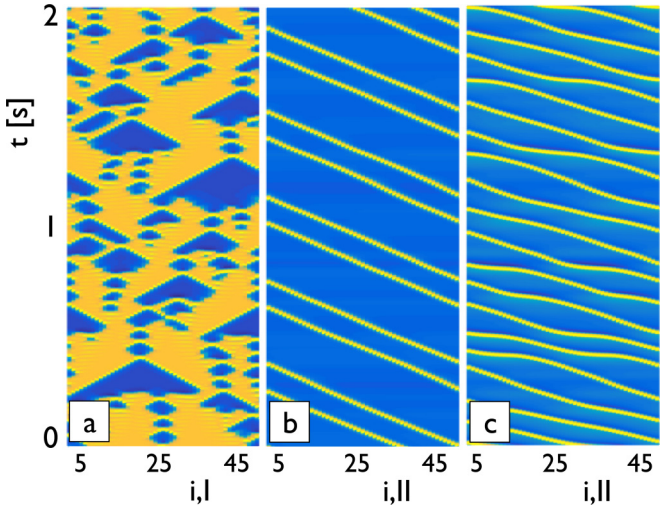

FIG. 11. Spatiotemporal chaos in layer I (a) synaptically influences the double pulse pattern in layer II for a synapse strength of $g = 0.004$ mS/cm^2 (b) and for the standard value $g = 0.01$ mS/cm^2 (c). The two pulses in layer II result from the collapse of STC to a double pulse.

the other half shows a collapse to rest with an average transient lifetime of 53.4 ± 52.5 s. The increase in lifetime for larger coupling strength is consistent with longer sequences of small scale patterns in STC, where small neuron groups alternate between firing and short periods of rest. Such small scale repetitive patterns are visible in Fig. 9(b), but they last longer for higher g. Delay in collapse through small-scale patterns was also reported for an isolated layer of neurons [17], in which the average lifetime of STC increased exponentially with the applied current parameter I.

D. Chaos in layer I maximizes distance between multiple erratic pulses in layer II

STC in layer II collapses also to multiple pulses, while layer I is in the STC state [Sec. III C, Fig. 9(c)]. The resulting presynaptic STC input can yield pulse distance maximization in layer II. Figure 11 reveals a rather steady pulse separation for very weak synapse strengths ($g = 0.004$ mS/cm^2), and an increase in pulse separation to a distance maximized double pulse for weak synapse strength ($g = 0.01$ mS/cm^2). This finding is in contradiction to pulse merging in the absence of synaptic coupling, $g = 0$, where the trailing pulse accelerates to merge with the leading pulse to cause chaos initiation [26,48].

Figure 12 shows representative time evolutions of pulse distances, d_P, that were calculated for synapse strengths within the interval [0.00,0.02] mS/cm^2 with a resolution of 0.001 mS/cm^2. A similarly fast increase in pulse distance is observed for $g = 0.008$ mS/cm^2 and larger values. Smaller coupling strengths yield a more gradual increase in pulse distance over time. For $g \leqslant 0.004$ mS/cm^2, no change in pulse distance was observed on such time scales [100 s, Fig. 12(b)], since chaos is reinitiated from the pulses on a faster time scale

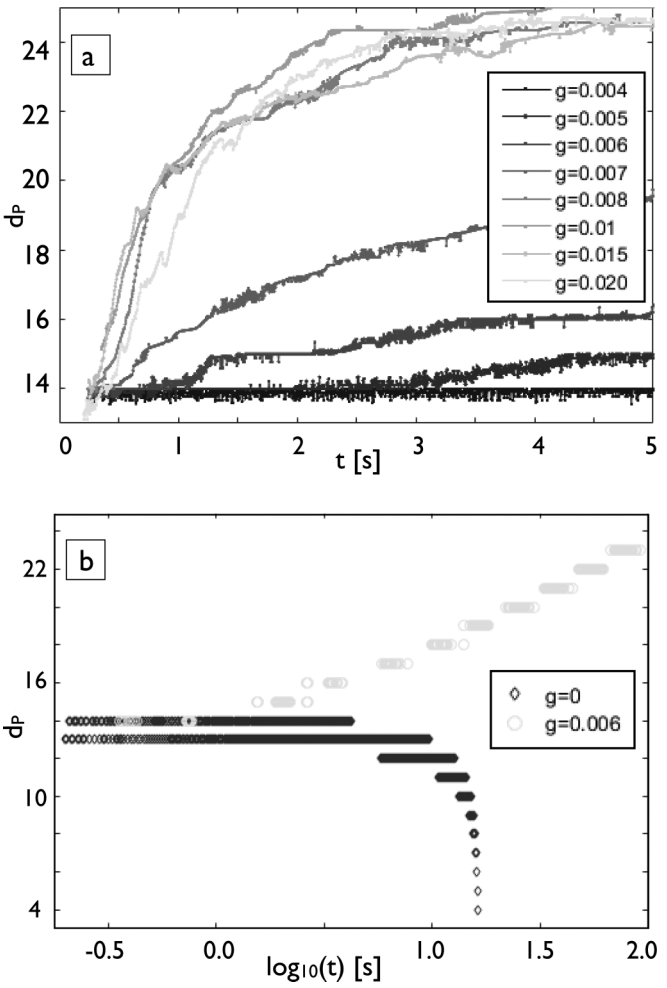

FIG. 12. Time evolution of pulse distance d_P (in layer II) as a response to STC input from layer I for varying synapse strengths g ($N = 50$ neurons; Fig. 11). (a) The pulse distance for each coupling strength was calculated from interpolation of pulse peaks over a time interval of 5 ms, and then averaged for nine different STC realizations in layer I. No change in pulse distance is observed for $g \in \{0.001,0.002,0.003,0.004\}$ mS/cm^2; only the curve for $g = 0.004$ mS/cm^2 is included. (b) Long-term simulation over 100 s for a case of slow pulse distance maximization ($g = 0.006$ mS/cm^2) and for the case of pulse merging in the absence of synaptic input ($g = 0$).

(Sec. III F). Fast pulse distance maximization is observed for coupling strengths for which STC in layer I can excite a neuron in layer II from the rest state (Fig. 4) to form a stripe [43].

The erratic multipulse pattern in layer II exists until STC collapses in layer I; for an early collapse, pulse distances increase but might not be maximized. For a collapse of STC to the rest state, layer II becomes an isolated diffusive layer with multiple traveling pulses that will eventually exhibit pulse merging [26] and chaos reinitiation. For a collapse of STC to a narrow pulse, the pulse distance maximization process in layer II stops, and eventually chaos is reinitiated from one of the pulses. For a collapse of STC to a wide pulse, chaos is immediately reinitiated in layer II, discussed further in Sec. III E.

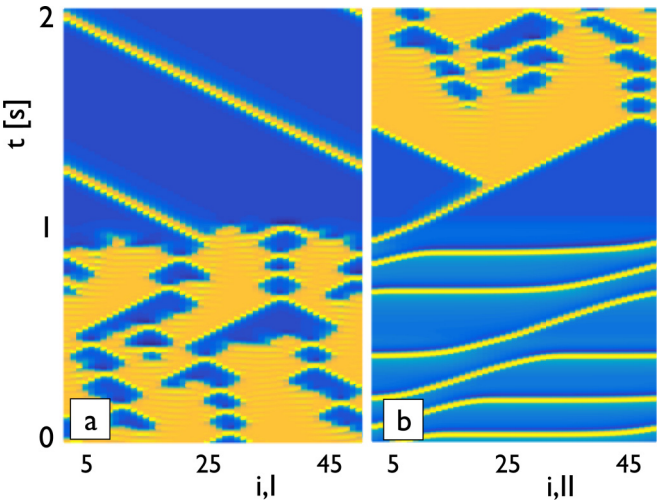

FIG. 13. Simultaneous change of dynamics in layers I and II ($g = 0.01$ mS/cm^2): the collapse of spatiotemporal chaos to a wide pulse in layer I (a), and reinitiation of spatiotemporal chaos from the erratic pulse pattern in layer II (b).

E. Wide pulse in layer I, chaos reinitiation in layer II

The collapse of STC to a wide pulse in layer I causes a simultaneous reinitiation of STC from the erratic pulse state in layer II. Figure 13 shows that the erratic pulse pattern in layer II ceases with the onset of the wide pulse in layer I, and the resulting constant presynaptic input disturbs the (driven) narrow pulse in layer II to quickly start chaos. The collapse of STC to a wide pulse presents a substantial reduction in presynaptic input to the erratic pulse pattern in layer II, an apparent requirement for destabilizing the pulse into chaos reinitiation.

Numerical simulations show that simultaneous chaos reinitiation exists for a range of synapse strengths, $g \in [0.007, 0.012]$ mS/cm^2, when varying g within the interval of $[0.00, 0.02]$ mS/cm^2 with a resolution of 0.001 mS/cm^2; the time delay between collapse in layer I and onset of reinitiation in layer II is between 500 and 150 ms, with the minimum delay at an intermediate coupling strength. For larger g values the erratic pulse develops into a (driven) wide pulse, and for smaller values, $g \in [0.004, 0.006]$ mS/cm^2, the erratic pulse develops into a (driven) narrow pulse with no chaos reinitiation following in either case [47].

The wide pulse in layer I is asymptotic (Fig. 13), but STC in layer II will eventually collapse. Only a collapse to rest and to the wide pulse is observed, no collapse to the narrow pulse. The collapse to the narrow pulse is prevented through an immediate chaos reinitiation induced by the synaptic input from the wide pulse (Sec. III G). The collapse to the wide pulse is asymptotic.

Figure 14 shows that reinitiation of STC also exists from an erratic multiple pulse pattern in layer II. The reinitiated STC pattern exhibits a transient, almost perfect (180 degree) rotational symmetry, when the erratic pulses lived long enough that pulse distances were maximized (Sec. III D). The synaptic input I^{syn} on each pulse is (almost) identical in the discrete network, as is the diffusive coupling in the neighborhood of the pulse when distance maximized. The symmetry parameter,

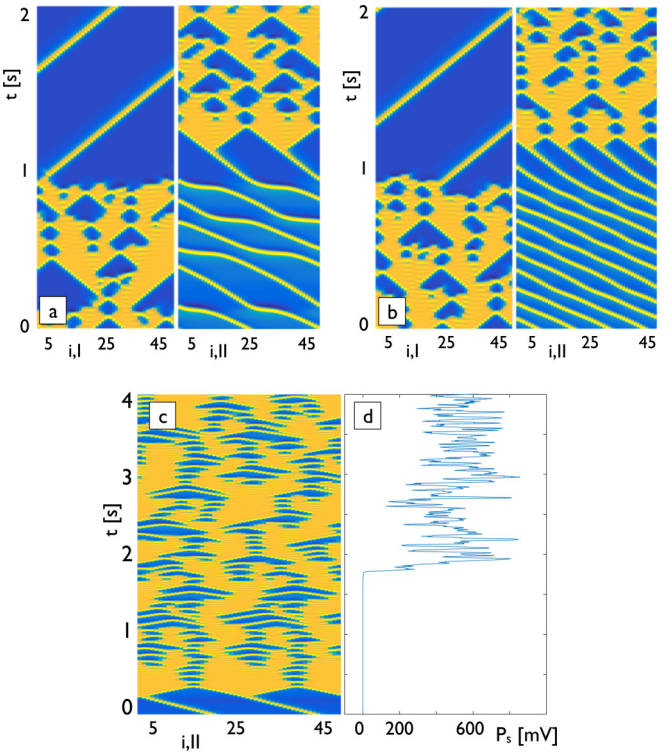

FIG. 14. Reinitiation of STC in layer II from an erratic double pulse (a) and an erratic quadruple pulse (b), analogous to Fig. 13. Spatiotemporal dynamics in layer II (c) and the corresponding symmetry parameter $P_s = \sum_{i=1}^{25} \|V_i - V_{i+25}\|$ (d) after chaos reinitiation from a distance maximized double pulse in a layer of $N = 50$ neurons and $g = 0.01$ mS/cm^2.

$P_s = \sum_{i=1}^{25} \|V_i - V_{i+25}\|$, reveals that this symmetry is lost after about 2 s of STC [Figs. 14(c) and 14(d)], a typical time scale for the parameters under study.

A slight trend toward longer average lifetimes for reinitiated STC is observed [44], although three very short lifetimes exist. These quick collapses happen during the symmetric phase of STC when pulse distances were maximized; they point to a smaller effective network size for symmetric STC.

F. Chaos in layer I, chaos reinitiation in layer II

Rare events with a substantial reduction in activity are inherent in STC dynamics and yield chaos reinitiation in layer II while STC is active in layer I. Figure 15 shows reinitiation of chaos when STC in layer I almost collapses and momentarily exhibits activity similar to a wide pulse (Sec. III E). For $g = 0.01$ mS/cm^2, such a reduction to few active neurons is required for destabilizing the erratic pulse in layer II into chaos reinitiation. Near collapses like that are increasingly rare for larger layers, since the mean lifetime of STC grows exponentially with the number of neurons.

More active neurons (and consequently less rare momentary STC patterns) can also accomplish such an overall substantial reduction in presynaptic input, if the synapse strength g is clearly reduced. Representative space-time patterns (Fig. 16) reveal that few neurons (covering several pulse widths) in layer I are active at the onset of chaos reinitiation when the

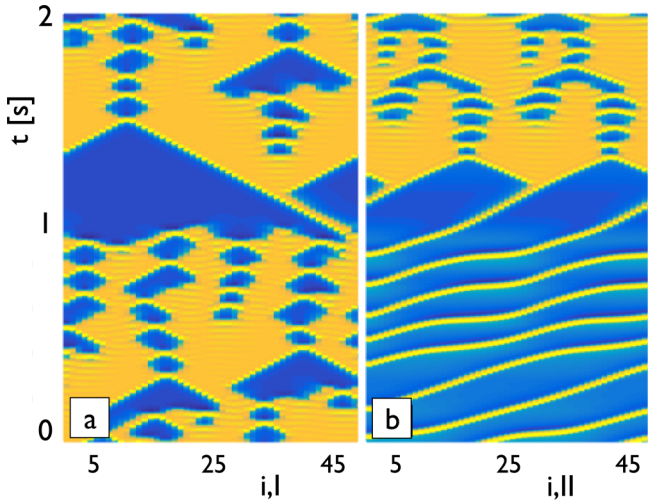

FIG. 15. A rare event of chaos reinitiation from an erratic pulse in layer II (b) through the synaptic STC input from layer I (a) at $g = 0.01$ mS/cm^2, observed once in about 200 simulations.

synapse strength is reduced by 70%; a reduced neuron activity is less obvious when g is decreased by about 80%. Chaos reinitiation occurs almost instantaneously for even smaller g, $g \in [0.0005, 0.0019]$ mS/cm^2, which indicates that no rare event is required for chaos to start. As g approaches zero, chaos reinitiation is absent and the traveling pulse in layer II becomes asymptotic. Figure 16(d) shows that the reduction in presynaptic input ($I_p = g \sum_{j=1}^{N} s_{ji}^{\mathrm{I,II}}$) near the onset of chaos reinitiation is similar for a range of coupling strengths, whether the reinitiation is from STC in layer I or from a wide pulse (Sec. III E). Increasingly rare events consisting of fewer active neurons are required for chaos reinitiation at larger coupling strengths.

G. Chaos collapses first in layer I

When STC collapses in layer I (while active in layer II), it typically [45] reaches the rest state or the single (narrow or wide) pulse state, which are asymptotic states. Upon collapse to rest, the presynaptic input vanishes and transient STC in layer II follows the escape routes discussed for an isolated diffusive layer (Sec. II, Refs. [17,26]). Upon collapse to a single pulse, the presynaptic input ($\sum_{j=1}^{N} s_{ji}^{\mathrm{I,II}}$) is constant; resulting fluctuations in the average lifetime of STC show no clear trend with coupling strength g.

STC in layer II will eventually collapse to the rest state or to a driven narrow/wide pulse state [45], while layer I continues to exhibit a traveling pulse. For a collapse to the rest state, the constant synaptic input from the pulse in layer

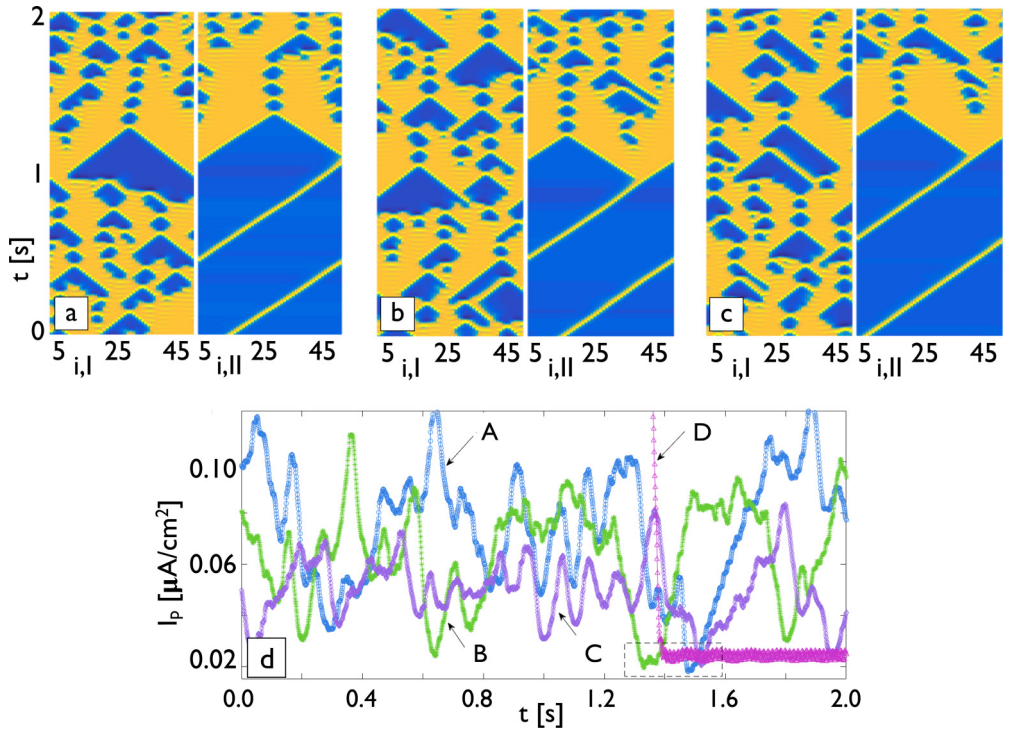

FIG. 16. Chaos reinitiation from a (driven) narrow pulse in layer II (right pattern) through the synaptic input of STC in layer I (left pattern) for tiny synaptic coupling strength: (a) $g = 0.003$ mS/cm^2 (case A), (b) $g = 0.0025$ mS/cm^2 (case B), and (c) $g = 0.002$ mS/cm^2 (case C). The synaptic coupling is small enough that the pulse in layer II is not erratic, traveling with a rather constant speed. Only a fraction (2 s) of the simulation time near the time of chaos reinitiation is shown. (d) Presynaptic input ($I_p = g \sum_{j=1}^{N} s_{ji}^{\mathrm{I,II}}$) near the time of chaos reinitiation. The time interval represents about 1.5 s before and about 0.5 s after chaos reinitiation, slightly off centered within the box for clarity. The STC dynamics in layer I is identical for all three cases, and chaos reinitiation occurs after 33.7 s of simulation time for case A, after 7.3 s for case B, and after 3.6 s for case C. While the particular value of reinitiation time depends on the STC realization, increasing reinitiation times reflect that the required reduction in presynaptic input is more rare. The reduction of I_p when STC collapses to a wide pulse in I (Sec. III E, $g = 0.01$ mS/cm^2) is shown for comparison (case D).

I results in a periodic stripe pattern in layer II for g above the respective critical coupling strengths (Fig. 4). The periodic firing is in contrast to the aperiodic firing pattern for STC synaptic input, discussed in Sec. III A. For the collapse to a pulse ($g = 0.01$ mS/cm^2), we find that STC is immediately reinitiated from a single or double narrow pulse as long as there is a wide or double narrow pulse in layer I. Consequently the collapse to a narrow pulse can not be observed if there is a wide pulse in layer I. The collapse to the narrow pulse is asymptotic, if there is a narrow pulse in layer I. The collapse to a wide pulse is always asymptotic, independent of the type of pulse in layer I.

The robustness of chaos reinitiation under varying synaptic strength ($g \in [0.00, 0.02]$ mS/cm^2 with a resolution of 0.001 mS/cm^2) is explored numerically by initializing the dynamics in layers I and II with all combinations of (wide, narrow, or double narrow) pulse solutions: the (driven) wide pulse in layer II is asymptotic for every pulse type in layer I. The (driven) narrow pulse in layer II is asymptotic for weak synaptic coupling below ($g = 0.006$; 0.007; 0.012) mS/cm^2, if the synaptic input is from a (double narrow; wide; narrow) pulse; otherwise, pulse solutions in layer II are not asymptotic and chaos is initiated "quickly."

IV. SWITCHING OF PATTERNS IN A SYSTEM WITH TWO-WAY SYNAPTIC COUPLING BETWEEN LAYERS I AND II

Two identical layers of ML neurons are now bidirectionally coupled such that every neuron in each layer is synaptically coupled to every neuron in the other layer [Eq. (1)]. All synapses have identical strength g, which implies that the network is symmetric under the exchange of layers I and II. This symmetry leads to novel switching sequences, the swapping of states between layers as well as the simultaneous chaos reinitiation; it excludes switching sequences from Sec. III that follow from an isolated layer.

Figure 17 shows a (preliminary) overview of observed sequential pattern switching. When both layers are initially in a state of transient STC, one of the layers will eventually collapse to the rest state or to a pulse state. The coupling symmetry allows two options: a collapse to rest results in a stripe pattern in one layer and STC in the other layer, and a collapse to either of the pulses results in the erratic pulse pattern in one layer and STC in the other layer. Secondary transitions are based on the further collapse of STC: Low presynaptic input terminates the

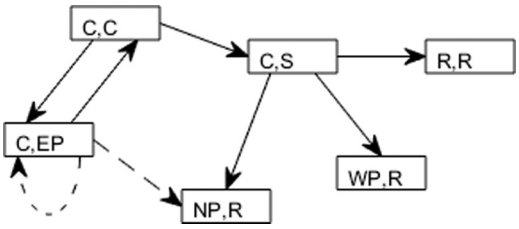

FIG. 17. Summary sketch ($g = 0.01$ mS/cm^2) for switching behavior in the case of two-way synaptic coupling between layers I and II. Arrows mark transitions to states [A,B], and dashed arrows to symmetrically equivalent states [B,A]; e.g., [C,EP] is mapped onto [EP,C]. Further information in Fig. 3.

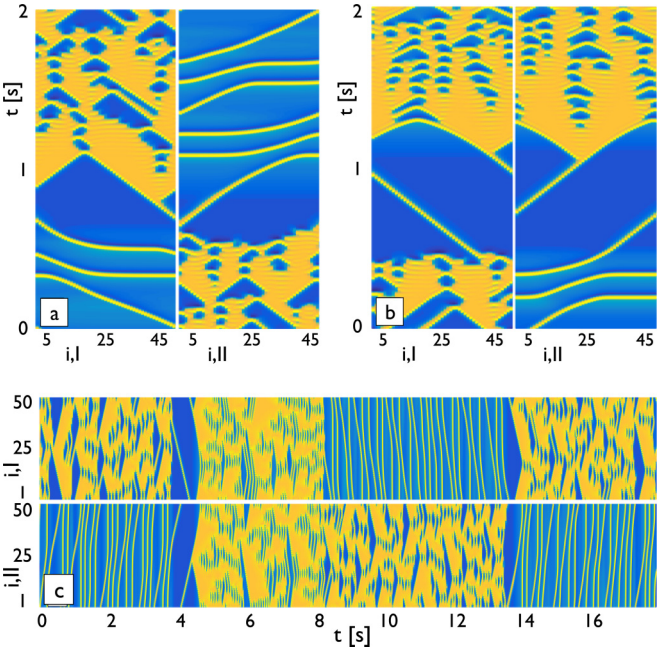

FIG. 18. Spatiotemporal dynamics for two-way synaptic coupling ($g = 0.01$ mS/cm^2) between layers I and II. Example for (a) a swapping event, (b) a simultaneous chaos reinitiation, and (c) a fast switching sequence.

stripe pattern upon collapse of STC, resulting in asymptotic patterns comprised of one inactive neuron layer and another layer with either a wide pulse, a narrow pulse, or no neuron activity. Three outcomes are possible when STC collapses while coexisting with an erratic pulse pattern: for a collapse to the rest state, the erratic pulse pattern becomes a traveling narrow pulse, which is asymptotic; for a collapse to a wide pulse, immediate swapping of STC and erratic pulse occurs [Fig. 18(a)], and for a collapse to a narrow pulse, immediate chaos reinitiation in both layers is observed [Fig. 18(b)].

A rare example with frequent switches is given in Fig. 18(c). After about 400 s during which one layer was in the STC state and the other layer was in an erratic pulse state, simultaneous chaos reinitiation occurs, followed by a collapse of STC to an erratic pulse in one layer, and then followed by a swapping of STC and erratic pulse pattern, all within about 12 s.

Whenever STC coexists with an erratic pulse, these states swap between the layers, if STC collapses to a wide pulse [Fig. 18(a)]. The synaptic input from this (driven) wide pulse changes the erratic pulse to a (driven) narrow pulse, which is quickly destabilized to reinitiate STC; STC in turn transforms the wide pulse into an erratic pulse pattern. This swapping process is analogous to chaos reinitiation discussed in Sec. III E, except that the two-way synaptic coupling allows for an erratic pulse pattern before and after the swapping. The number of pulses in the erratic pulse pattern before and after swapping need not be identical, since STC can collapse to multiple pulses at any collapse within a switching sequence.

Whenever STC coexists with an erratic pulse, chaos reinitiation occurs in both layers, if STC collapses to a narrow pulse [Fig. 18(b)]. The synaptic input from the (driven) narrow pulse changes the erratic pulse to a (driven) narrow pulse. The mutual synaptic input destabilizes each (driven) narrow pulse

to reinitiate STC in both layers. The timing of chaos reinitiation is rather simultaneous, with a slightly earlier reinitiation in the layer proceeded by the erratic pulse pattern.

V. CONCLUSION

Earlier studies [17,26] of a single-ring network (layer) of diffusively coupled, identical, excitatory Morris-Lecar neurons report that spatiotemporal chaos (STC) collapses to either a rest state with no neuron activity, or to a propagating pulse. The sudden, system intrinsic collapse points to the existence of a chaotic saddle in the presence of multiple attractors; the average lifetime of STC increases exponentially with system size, which is typical for the escape from a saddle [1,12]. We synaptically couple two such neuron layers and find irregular, nonpredictable, system-intrinsic switching sequences of spatiotemporal patterns within and between the layers.

Within a layer, STC frequently switches to a sustained state where all neurons become momentarily active at irregular times until an eventual collapse to neuron inactivity, or, STC switches to a pattern of erratic pulse propagation before reinitiation of STC. More complex transitions are observed between layers. For example, a sudden substantial reduction of neuron activity in one layer induces pulse destabilization to STC reinitiation in the other layer. Such activity reduction may be caused by a collapse of STC to a wide pulse, by a rare event of low activity within STC, or by an overall reduction in coupling strength between the layers. These phenomena lead to a spontaneous swap of STC and traveling pulse state between layers when every neuron in one layer is synaptically coupled to every neuron in the other layer (two-way coupling).

The asymptotic states of the coupled two-layer system reflect all combinations of rest and pulse states. In the case of one-way synaptic coupling, where every neuron in layer I is coupled to every neuron in layer II, each asymptotic state is reached on a definite path that includes two or three observed switches from the initial STC state; the time between switches is irregular and shows the typical exponential distribution for escape from a saddle. This finding is consistent with the existence of heteroclinic orbits (chain of saddles [8]) for the coupled system. One way-coupling has applications in projections between neuronal layers in the brain or, e.g., the visual system; it also serves as model to better understand switching in the case of two-way synaptic coupling. For the two-way synaptic coupling (preliminary results), an asymptotic state can be reached via an arbitrary number of switches from the initial STC state with irregular times between switches. This finding could also be consistent with the existence of a chaotic saddle that contains different space-time patterns, introduced in Ref. [32]. Two-way coupling has applications in interacting subnetworks in the brain or in complex network models per se. Further studies are necessary to clarify the details of the saddle properties.

For a collapse of STC to multiple pulses, we observe that pulse distances are maximized through synaptic STC input. This is in contrast to the merging of pulses in the absence of synaptic input. Distance maximized pulses exhibit a transient, high degree of spatial symmetry in STC upon chaos reinitiation.

Spontaneous transitions are reported in the context of neurological disease associated with disruptions of neurological rhythms [3]. Reproducible transient behavior is thought to play an integral role in perceptual phenomena associated with stimuli and in cognitive function, observed as sequential switching of neuron activity among different neurons or neuron groups from one metastable state to another [2,8]. The role of chaotic saddles for such transitions is not explored.

[1] T. Tél and Y. C. Lai, Phys. Rep. **460**, 245 (2008).
[2] O. Mazor and G. Laurent, Neuron **48**, 661 (2005).
[3] T. J. Kaper, M. A. Kramer, and H. G. Rotstein, Chaos **23**, 046001 (2013).
[4] H. Fujii and I. Tsuda, Neurocomputing **58-60**, 151 (2004).
[5] M. A. Dahlem and E. P. Chronicle, Prog. Neurobiol. **74**, 351 (2004).
[6] M. C. Cross and P. C. Hohenberg, Rev. Mod. Phys. **65**, 851 (1993).
[7] S. Kraut and U. Feudel, Phys. Rev. E **66**, 015207(R) (2002).
[8] M. I. Rabinovich and P. Varona, Front. Comp. Neurosci. **5**, 24 (2011).
[9] S. Jahnke, R-M. Memmesheimer, and M. Timme, Phys. Rev. Lett. **100**, 048102 (2008).
[10] R. Zillmer, N. Brunel, and D. Hansel, Phys. Rev. E **79**, 031909 (2009).
[11] S. Luccioli and A. Politi, Phys. Rev. Lett. **105**, 158104 (2010).
[12] Y. Lai and T. Tél, *Transient Chaos: Complex Dynamics on Finite Time Scales* (Applied Mathematical Sciences, Springer, New York, 2011).
[13] B. Hof, J. Westerweel, T. M. Schneider, and B. Eckhardt, Nature **443**, 59 (2006).
[14] A. Wacker, S. Bose, and E. Schöll, Europhys. Lett. **31**, 257 (1995).
[15] M. C. Strain and H. S. Greenside, Phys. Rev. Lett. **80**, 2306 (1998).
[16] R. Wackerbauer and K. Showalter, Phys. Rev. Lett. **91**, 174103 (2003).
[17] K. Keplinger and R. Wackerbauer, Chaos **24**, 013126 (2014).
[18] S. Houghton, E. Knobloch, S. Tobias, and M. Proctor, Phys. Lett. A **374**, 2030 (2010).
[19] D. Stahlke and R. Wackerbauer, Phys. Rev. E **80**, 056211 (2009).
[20] D. Stahlke and R. Wackerbauer, Phys. Rev. E **83**, 046204 (2011).
[21] D. Ruelle, *Chaotic Evolution and Strange Attractors* (Cambridge University Press, New York, 1989).
[22] M. P. Fishman and D. A. Egolf, Phys. Rev. Lett. **96**, 054103 (2006).
[23] J. P. Crutchfield and K. Kaneko, Phys. Rev. Lett. **60**, 2715 (1988).
[24] R. Wackerbauer and S. Kobayashi, Phys. Rev. E **75**, 066209 (2007).
[25] S. Yonker and R. Wackerbauer, Phys. Rev. E **73**, 026218 (2006).
[26] J. Lafranceschina and R. Wackerbauer, Chaos **25**, 013119 (2015).

[27] R. Wackerbauer, H. Sun, and K. Showalter, Phys. Rev. Lett. **84**, 5018 (2000).
[28] H. Kori and Y. Kuramoto, Phys. Rev. E **63**, 046214 (2001).
[29] M. Timme, F. Wolf, and T. Geisel, Phys. Rev. Lett. **89**, 154105 (2002).
[30] F. Schittler Neves and M. Timme, Phys. Rev. Lett. **109**, 018701 (2012).
[31] H-L. Zou, Y. Katori, Z-C. Deng, K. Aihara, and Y-C. Lai, Chaos **25**, 103109 (2015).
[32] G. Ansmann, K. Lehnertz, and U. Feudel, Phys. Rev. X **6**, 011030 (2016).
[33] C. Morris and H. Lecar, Biophys. J. **35**, 193 (1981).
[34] K. Tsumoto, H. Kitajima, T. Yoshinaga, K. Aihara, and H. Kawakami, Neurocomputing **69**, 293 (2006).
[35] A. Destexhe, Z. F. Mainen, and T. J. Sejnowski, J. Comp. Neurosci. **1**, 195 (1994).
[36] I. Song and R. L. Huganir, Trends Neurosci. **25**, 578 (2002).
[37] G. B. Ermentrout and D. H. Terman, *Mathematical Foundations of Neuroscience*, Vol. 64 (Springer, New York, 2010).
[38] D. Feldmeyer and J. Lübke, *New Aspects of Axonal Structure and Function* (Springer e-Books, Springer, New York, 2010).
[39] D. M. Durand, E.-H. Park, and A. L. Jensen, Philos. Trans. Roy. Soc. B **365**, 2347 (2010).
[40] R. Wackerbauer, Phys. Rev. E **76**, 056207 (2007).
[41] Brief disturbances to the stripe pattern are observed at their onset when a pair of pulses traveling in opposite directions annihilate each other to generate a rest state, or when layer I initiates a stripe before all postsynaptic neurons reached their rest state upon collapse of STC. Such transient disturbances persist longer for stronger synapses due to shorter time intervals between stripes.
[42] For an excited presynaptic neuron, $1+\exp(\cdot)\approx 1$ in Eq. (7), and $s_{ji}^{\mathrm{I,II}}=\frac{\alpha T_m}{\alpha T_m+\beta}$, which is about 0.85 for the parameters in Table I. For an inactive presynaptic neuron, $1+\exp(\cdot)\gg 1$, and $\dot{s}_{ji}^{\mathrm{I,II}}\approx-\beta s_{ji}^{\mathrm{I,II}}$, resulting in $s_{ji}^{\mathrm{I,II}}\to 0$.
[43] Synaptic input can locally delay excitation to generate a fast propagating pulse instead of simultaneous neighboring neuron excitations (partial stripe). If subsequent stripe formation happens quickly, neurons involved in the fast propagating pulse are still in the refractory period and don't contribute to the stripe. This changes the distance between pulses that start at the free ends of the partial stripes (Sec. III B). The mechanisms for slow pulse distance maximization require further study.
[44] Reinitiated STC from a double pulse has a lifetime of 206 ± 178 s (19 cases) when STC was reinitiated before pulse distances were maximized, and similarly 186 ± 151 s (14 cases) when STC was reinitiated from distance maximized pulses but collapsed after symmetric STC was lost. For comparison, STC lifetimes are 166 ± 132 s (50 cases) in the presence of a wide pulse in layer I, 36 ± 42 s for STC in layer I (50 cases), and 131 ± 136 s (100 cases) for $g=0$. Otherwise, $g=0.01\,\mathrm{mS/cm^2}$. Further statistics is required for reinitiated STC.
[45] In rare cases, STC in layer I collapses to two (multiple) narrow pulses. The diffusive interaction of multiple pulses leads to pulse merging on long time scales [26] and then reinitiation of STC.
[46] G. Benettin, L. Galgani, and J.-M. Strelcyn, Phys. Rev. A **14**, 2338 (1976).
[47] Chaos reinitiation is observed for very small synapse strength ($g\leqslant 0.003\,\mathrm{mS/cm^2}$) and happens almost concurrently with the collapse in layer I. The delay time is about 20 ms ($g=0.002$ and $0.003\,\mathrm{mS/cm^2}$), or negative for $g=0.001\,\mathrm{mS/cm^2}$. Leftover activity from STC collapse and ongoing STC activity in the latter case, together with low coupling strength provide the necessary reduction in presynaptic input for chaos reinitiation (Sec. III F).
[48] J. Christoph, M. Eiswirth, N. Hartmann, R. Imbihl, I. Kevrekidis, and M. Bär, Phys. Rev. Lett. **82**, 1586 (1999).